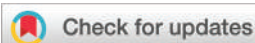


## PAPER

Cite this: *Nanoscale*, 2021, **13**, 11232

## Borate-driven ionic rectifiers based on sugar-bearing single nanochannels†

Vanina M. Cayón, <sup>‡a</sup> Gregorio Laucirica, <sup>‡a</sup> Yamili Toum Terrones, <sup>a</sup>  
M. Lorena Cortez, <sup>a</sup> Gonzalo Pérez-Mitta, <sup>a</sup> Jun Shen,<sup>b</sup> Christian Hess,<sup>b</sup>  
María Eugenia Toimil-Molares,<sup>c</sup> Christina Trautmann,<sup>c,d</sup>  
Waldemar A. Marmisollé <sup>\*a</sup> and Omar Azzaroni <sup>\*a</sup>

Recently, much scientific effort has been centered on the control of the ionic transport properties of solid state nanochannels and the rational design and integration of chemical systems to induce changes in the ionic transport by means of interactions with selected target molecules. Here, we report the fabrication of a novel nanofluidic device based on solid-state nanochannels, which combines silane chemistry with both track-etched and atomic layer deposition (ALD) technologies. Nanodevice construction involves the coating of bullet-shaped single-pore nanochannels with silica (SiO<sub>2</sub>) by ALD and subsequent surface modification by reaction between silanol groups exposed on pore walls and *N*-(3-triethoxysilylpropyl)-gluconamide, in order to create a gluconamide-decorated nanochannel surface. The formation of a bor-ester derivative resulting from the selective reaction of borate with the appended saccharides leads to important changes in the surface charge density and, concomitantly, in the iontronic properties of the nanochannel. Furthermore, we propose a binding model to rationalize the specific interaction saccharide–borate in the surface. Besides, this unique nanodevice exhibits a highly selective and reversible response towards borate/fructose exposure. On the basis of the surface charge variation resulting from borate binding, the nanochannel can reversibly switch between “ON” and “OFF” states in the presence of borate and fructose, respectively. In addition, this work describes the first report of the functionalization of PET/SiO<sub>2</sub> nanochannels by the ALD technique. We believe that this work provides a promising framework for the development of new nanochannel-based platforms suitable for multiple applications, such as water quality monitoring or directed molecular transport and separation.

Received 28th October 2020,

Accepted 17th May 2021

DOI: 10.1039/d0nr07733j

rsc.li/nanoscale

## Introduction

Over the last few years, solid-state nanochannels (SSNs) have been extensively studied and have revolutionized both basic and applied research.<sup>1–3</sup> Most of the attention on these systems is owing to their similarity to biological ion channels.<sup>4,5</sup> In general, ion channels in nature are membrane proteins that employ a delicate concatenation of both confor-

mational and electrostatic changes that allow them to respond to different stimuli and to regulate ionic transport through biological membranes.<sup>6</sup> Biological channels perform crucial functions for cells including the regulation of physiological parameters such as ionic flow, electric potential, and molecular transport across the cell membranes. Inspired by these unique functional features of biological ion channels, scientists have begun to develop and study fully abiotic biomimetic nanochannels with similar functional capabilities as constituent elements of biosensors, nanofluidic devices, and artificial molecular filtration systems.<sup>7–21</sup> To achieve this goal, the development of synthetic nanochannels combining nanofluidic fabrication techniques with different surface modification procedures was propelled at the same time. Moreover, surface modification techniques promote the integration of different functional groups within nano-architectures<sup>22–26</sup> that confer them specific responses under a wide variety of stimuli such as pH changes, temperature, light, electrochemical potential<sup>27,28</sup> and the presence of a particular analyte.<sup>29–40</sup> In this context, the development of SSNs in polymer membranes

<sup>a</sup>Instituto de Investigaciones Fisicoquímicas Teóricas y Aplicadas (INIFTA), Departamento de Química, Facultad de Ciencias Exactas, Universidad Nacional de La Plata, CONICET – CC 16 Suc. 4, 1900 La Plata, Argentina.

E-mail: azzaroni@inifta.unlp.edu.ar

<sup>b</sup>Eduard-Zintl-Institut für Anorganische und Physikalische Chemie, Technische Universität Darmstadt, Alarich-Weiss-Str. 8, Darmstadt, Germany

<sup>c</sup>GSF Helmholtzzentrum für Schwerionenforschung, 64291 Darmstadt, Germany

<sup>d</sup>Technische Universität Darmstadt, Materialwissenschaft, 64287 Darmstadt, Germany

†Electronic supplementary information (ESI) available. See DOI: 10.1039/d0nr07733j

‡These authors contributed equally to this work.

by the ion-track-etching technique is most widely used, mainly for its ability to build nanochannels with tailored geometry (*e.g.* conical, cylindrical or biconical) and size, which gives the channels unique iontronic characteristics such as rectifying diodes and field-effect transistors.<sup>41–45</sup> Additionally, shape asymmetry in SSNs leads to an asymmetry in the electric potential distribution inside the nanochannels; hence, an ionic-current rectification (ICR) effect across the channels is generated. In contrast to classical electrochemistry, solid-state nanochannel technologies are based on ions; the reason why the response is commonly referred to as iontronic output.<sup>46,47</sup> While the iontronic readout process requires instrumentation of lower complexity than other common sensing technologies, designing a system capable of specifically responding to target molecules is a real challenge.

Silica (SiO<sub>2</sub>)-based materials are versatile supporting materials as they are robust and stable, and at the same time, they are susceptible to surface post-grafting by chemical synthesis. Furthermore, there exists a vast library of molecules in the form of commercially available silanes, that allow the tuning of surface properties.<sup>48,49</sup> Regarding SSNs, new strategies to tailor the functionalities of the surface are always in need, and using SiO<sub>2</sub> to coat the surface of SSNs may enable the creation of unique inorganic/organic polymer composites. Among the different options to integrate SiO<sub>2</sub> within SSNs, atomic layer deposition (ALD) emerges as a powerful candidate technique. The ALD method is based on successive, separated, and self-terminating gas–solid surface reactions of two gaseous reactants yielding precise process control over film thickness and composition, and it has been extensively used to generate thin films on the surface of a variety of materials.<sup>50</sup> Recently, it has been demonstrated that it is possible to deposit different metal oxides on nanoporous structures by ALD, where TiO<sub>2</sub>, SiO<sub>2</sub>, and Al<sub>2</sub>O<sub>3</sub> films were success cases.<sup>51–53</sup> In this context, the ALD coating of track-etched nanochannels appears as an interesting approach as it allows the tuning of the diameter of track-etched nanochannels in a controlled manner without affecting their geometry.<sup>53–55</sup> Since the surface charge properties of the SSNs have a strong influence on the ionic transport properties of nanochannels, SiO<sub>2</sub> deposition and post-grafting procedures are expected to modify the rectification characteristics of bare track-etched polymer SSNs by introducing silanol groups (Si–OH) and derivatized silanes.

Silanization reactions are common synthetic procedures to functionalize different types of silica surfaces.<sup>55</sup> They involve hydrolysis and condensation stages of the target silane with the reactive silanol groups of the silica surface.<sup>56</sup> In this line, silanization procedures can be a good option to immobilize specific molecules on the silica hydroxyl-terminated surface of the SiO<sub>2</sub>-coated nanochannel. Although some examples of glass and alumina nanopore systems have been reported, post-functionalization studies of SiO<sub>2</sub>-coated single track-etched nanochannels remain scarce.<sup>57–64</sup>

Borate is a toxic chemical additive still being used in food production and processing, and its accumulation might cause serious effects to human health.<sup>65–67</sup> Besides, boric acid functionalized materials have appeared as intelligent platforms for

specific recognition and selective separation of *cis*-diol compounds, where the molecular recognition principle is based on the reversible covalent binding between boric acid ligands and *cis*-diol substances.<sup>68–71</sup> Many *cis*-diol compounds, such as dopamine, sugar and glycopeptides, have important biological and clinical significance and are the target of current metabolomics and proteomics research.<sup>72–79</sup> In this context, the development of ionic devices and nanofluidic elements responsive to borate ions could be of much interest in diverse fields.

Our attention in this work was focused on the specific reaction between saccharides and borate that results in the formation of boronate esters.<sup>80–83</sup> Previous works have taken advantage of this specific binding of saccharides to boronic acid receptors in order to build carbohydrate-stimuli responsive nanoarchitectures.<sup>58,84,85</sup> In that work, fructose was considered as a case of study since it shows a stronger binding affinity for borate ion compared with other saccharides.<sup>86</sup> On the other hand, from the wide range of possible glycosylated derivatives, *N*-(3-triethoxysilylpropyl)gluconamide (TESPG) was selected for the purpose of covalently grafting the pore walls and studying the effects of the borate–fructose interactions on the iontronic response. This glycosylated silane is a commercially available simple molecule and has been used successfully for different silica surface modifications.<sup>87,88</sup>

Here, we present a borate-responsive nanofluidic system by a combination of track-etched nanotechnology, atomic layer deposition, and wet silane chemistry. For this purpose, SiO<sub>2</sub>-coated bullet-shaped polyethylene terephthalate single nanochannels (PET/SiO<sub>2</sub> SSN) were modified by surface post-grafting functionalization with the glycosylated derivative TESPG, yielding a glycosylated abiotic nanochannel (PET/SiO<sub>2</sub>–Glu SSN). We proved that the specific reaction between gluconamide and borate, *i.e.* the boroester complex formation, occurs in the nanochannel leading to important changes in the surface charge density and, therefore, in its iontronic properties. Furthermore, fructose acts as a competitive effector and enables the removal of borate from the nanochannel surface, as revealed by abrupt changes in the SSN ion transport behavior. As a result, the fabricated nanodevice showed a reversible “ON/OFF” behaviour under successive exposure to borate ions and fructose, respectively. This, in turn, led to the development of a novel abiotic glycosylated nanochannel with a strong and sensitive iontronic response toward borate anions that act as receptors in the presence of gluconamide ligands on the nanochannel walls.

## Results and discussion

Asymmetric single bullet-shaped nanochannels with a base diameter of 900 nm were obtained by surfactant-assisted ion-track etching (Fig. S1†).<sup>89</sup> Then, the membranes were coated with SiO<sub>2</sub> by ALD resulting in small opening diameters ( $d_{\text{tip}}$ ) of ~30 nm as estimated from conductance measurements (see the ESI† for details). To characterize the PET/SiO<sub>2</sub> SSN response and optimize the ionic transport measurement con-

ditions,  $I$ - $V$  curves were measured at different ionic strength and pH values (Fig. S2(a) and (b)†). Finally, pH 7 and 100 mM KCl solutions were determined as the optimal experimental conditions to maximize the ionic current and rectification efficiency.

In terms of ionic transport properties, naked bullet-shaped PET SSNs show a cation-driven rectification owing to the interplay between the negative surface charge generated by the dissociation of carboxyl groups at neutral pH and the asymmetrical shape of the nanochannel (Fig. S3†).<sup>14</sup> In addition, the bullet geometry is expected to trigger the maximization of both the rectification efficiency and the channel conductance.<sup>12,90,91</sup> As shown in Fig. 1b, the SiO<sub>2</sub> coating on the tip side of bullet-shaped PET SSNs retains the cation-driven rectification regime of the unmodified nanochannel. As zeta-potential measurements reveal, the isoelectric point of surface grafted-SiO<sub>2</sub> nanoparticles varies according to the identity of the surface groups exposed to the solvent. In particular, SiO<sub>2</sub> without any extra surface functionalization appears negatively charged in aqueous solutions at pH > 3 due to the dissociation of different silanol groups.<sup>92,93</sup> Then, SiO<sub>2</sub>-coated nanochannels (PET/SiO<sub>2</sub> SSNs) were post-functionalized with

*N*-(3-triethoxysilylpropyl) gluconamide (TESPG) to produce PET/SiO<sub>2</sub>-Glu SSNs (see the Experimental section for details) as shown schematically in Fig. 1(a). Under these experimental conditions, TESPG is hydrolyzed and further condensed on the silica surface, as it occurs in typical silanization protocols. Once the grafting of saccharide moieties (Glu) has been performed, an evident change in the ionic transport from cation-driven rectification to ohmic behavior is evidenced (Fig. 1(c)). Covalent attachment of the gluconamide derivative provided by TESPG to the silica surface promotes a significant decrease in the surface charge of the nanochannel walls as ionizable silanol groups are partially replaced by neutral gluconamide groups.<sup>84</sup>

A standardized way to quantitatively analyze the changes in the iontronic response is by means of the rectification factor ( $f_{\text{rec}}$ ) since it is related to the surface charge density of the nanochannel (for more details, see the Experimental section).<sup>29</sup> In this regard, the functionalization with TESPG causes a change in  $f_{\text{rec}}$  from  $\sim -15$  (high rectification) to  $\sim 1$  (ohmic behavior) which is ascribed to the passivation of silanol groups by the covalent attachment of TESPG to give the glycol-derivatized SSN.

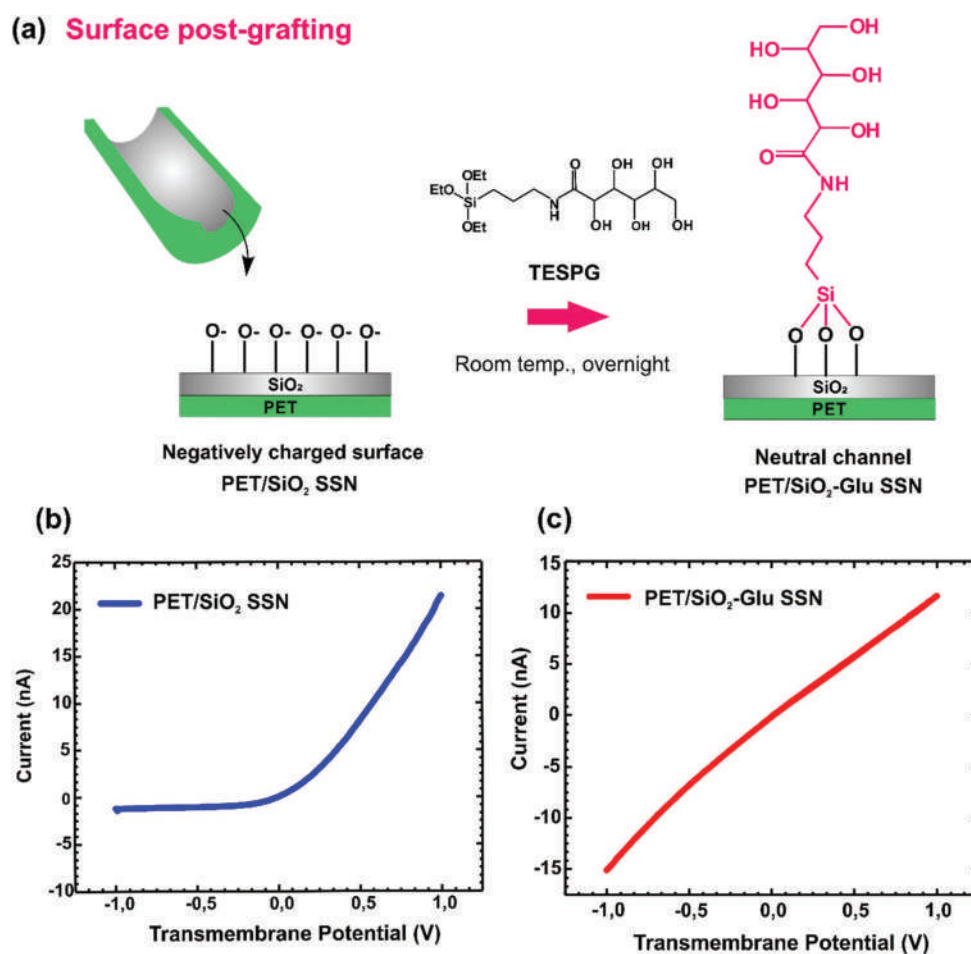


Fig. 1 (a) Scheme depicting the functionalization of a PET/SiO<sub>2</sub> coated nanochannel with TESPG to give the glycol-derivatized PET/SiO<sub>2</sub>-Glu SSN.  $I$ - $V$  curves (0.1 M KCl in 10<sup>-2</sup> M HEPES solution and pH = 7): (b) before (blue) and (c) after (red) derivatization.

In full agreement with the electrochemical data, the composition analysis of the PET/SiO<sub>2</sub>-Glu sample by XPS confirmed the successful functionalization of the surface. The spectrum presented in the ESI† is characterized by major peaks at 532.2, 399.7, 284.5, and 103.3 eV originating from O 1s, N 1s, C 1s, and Si 2p photoemission, respectively (Fig. S4†).

As mentioned above, saccharides act as ligands for the complexation of boric acid or borate, depending on the pH.<sup>82</sup> We kept away from acidic and basic pH values to prevent the possible degradation of borooesters and the silica matrix, respectively (Fig. S5†). Considering this background, the functionalized membranes were immersed in 100 mM boric acid solution at pH 7. Fig. 2(a) illustrates the putative reaction between borate and the saccharide-functionalized surface. The successful reaction of the PET/SiO<sub>2</sub>-Glu SSN with borate was confirmed by the recovery of the iontronic rectification (Fig. 2(b)) characterized by the increase and decrease of the conductance at +1 V and -1 V, respectively. This change in the response implies an enhancement in  $f_{\text{rec}}$  from  $\sim -1$  for the Glu-modified SSN (ohmic behavior) to  $\sim -7$  for the borate treated SSN, which is attributed to the generation of negatively charged sites in the nanochannel owing to the reaction with borate to form a grafted borooester surface. Appropriate control experiments were carried out to rule out an ionic strength effect due to the borate addition. With this goal in mind, the  $I$ - $V$  curves of the PET/SiO<sub>2</sub> samples before and after exposure to 100 mM boric acid solution were measured under the same conditions compared to those used for PET/SiO<sub>2</sub>-Glu SSN (Fig. S6†). The results revealed that the analyte concentration does not cause an important change in the ionic current for the saccharide-free sample, which reinforces the idea that the changes exhibited in the ionic transport are attributable to the interaction between the surface-confined saccharides and borate anions.

Also, it is important to emphasize that the system showed good stability in the current measurements (Fig. S7†).

Relative changes in  $f_{\text{rec}}$  ( $\Delta f_{\text{rec}}/f_{\text{rec}}^0$ ) triggered by the treatment with 100 mM boric acid solution for the PET/SiO<sub>2</sub> SSN and the PET/SiO<sub>2</sub>-Glu SSN are shown in Fig. 2(c). After the exposure of the gluconamide-modified membrane to boric acid, the ratio  $\Delta f_{\text{rec}}/f_{\text{rec}}^0$  increases more than 200 times compared with that of the PET/SiO<sub>2</sub> foil. Thus, the evident change in  $f_{\text{rec}}$  for the PET/SiO<sub>2</sub>-Glu SSN must be caused by the specific and effective interaction between the glycosylated residues of the SSN and borate ions to form borooesters on the nanochannel surface.

Changes caused by the different modification steps were also characterized by contact angle measurements. As shown in Fig. 2(d), the contact angle value decreases with the Glu-modification, from  $55^\circ \pm 3^\circ$  for SiO<sub>2</sub>-coated SSN to  $46^\circ \pm 2^\circ$  for PET/SiO<sub>2</sub>-Glu SSN, which agrees well with the replacement of silanol groups by hydroxyl moieties of the saccharide, thus increasing the surface hydrophilicity. Moreover, after the treatment with 100 mM boric acid solution, the contact angle measured under the same conditions became even lower ( $39^\circ \pm 2^\circ$ ), which shows again an increasing surface hydrophilicity behaviour due to the resulting negatively charged borooester groups. Also, a measurement of the contact angle was performed in a non-coated PET SSN as the control before the ALD process. A higher contact angle reveals a higher hydrophobicity of the surface in this case ( $72^\circ \pm 1^\circ$ ), which decreases when the tip side is coated with silica.

In order to shed light on the saccharide-borate interaction taking place in the confined environment of the nanofluidic device, the transmembrane  $I$ - $V$  curves of PET/SiO<sub>2</sub>-Glu SSN were measured in the presence of different boric acid concentrations. As can be seen in Fig. 3(a), there is an increase in the current at positive transmembrane voltages as boric acid con-

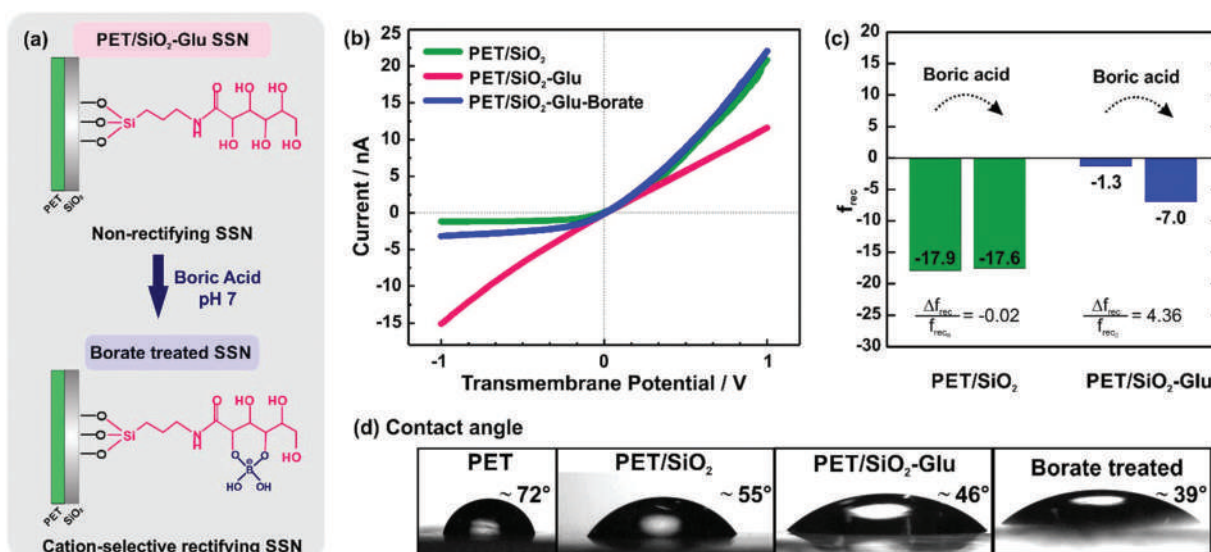
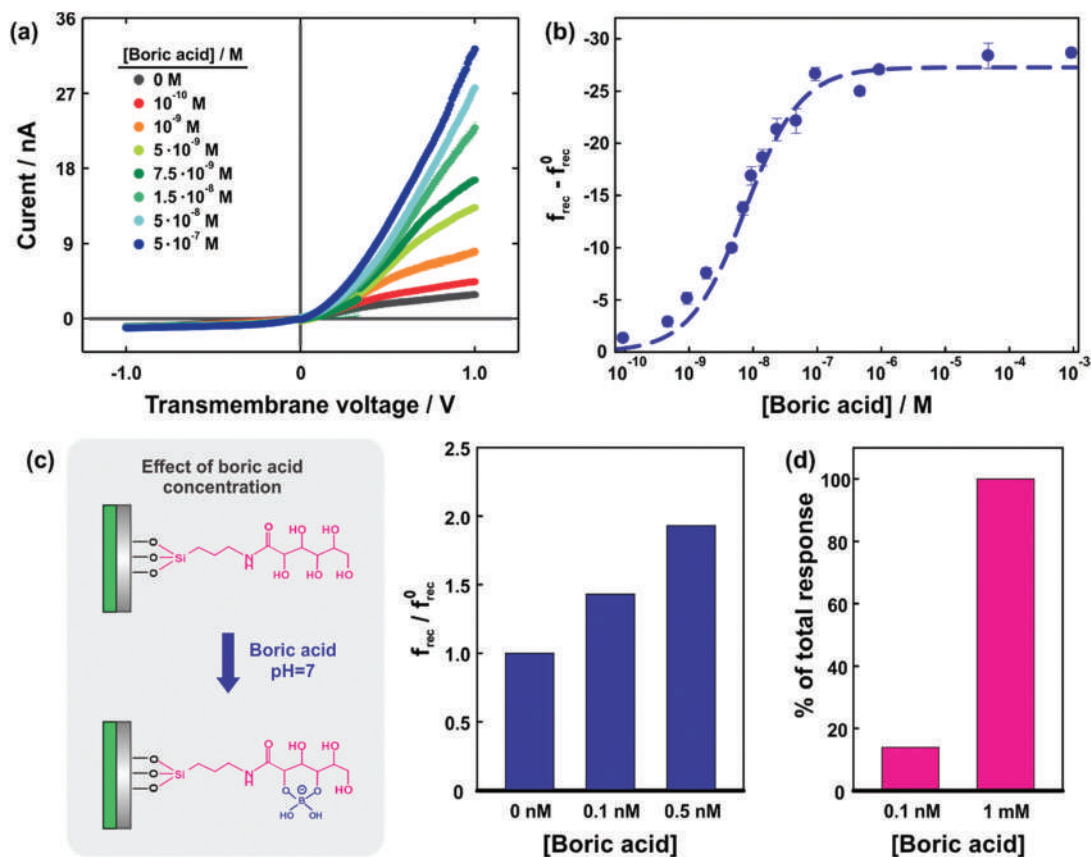


Fig. 2 (a) Representation of the borooester formation reaction between the gluconamide derivative and borate; (b)  $I$ - $V$  curves measured for PET/SiO<sub>2</sub> SSN (green), PET/SiO<sub>2</sub>-Glu SSN (pink), and PET/SiO<sub>2</sub>-Glu-boric acid treated (blue); (c) variations in the  $f_{\text{rec}}$  value of PET/SiO<sub>2</sub> and PET/SiO<sub>2</sub>-Glu before and after the exposure to boric acid. (d) Contact angle measurements at the different modification stages.



**Fig. 3** (a)  $I$ - $V$  curves recorded at different boric acid concentrations, from 0 to 100 mM (pH 7); (b) changes in  $f_{\text{rec}}$  for different boric acid analytical concentrations. The dashed line is the fitting to the binding model. (c) Relative change in the rectification factor ( $f_{\text{rec}}/f_{\text{rec}}^0$ ) before adding 0, 0.1 nM and 0.5 nM boric acid solution; (d) percentage of signal generated in the limit of detection (0.1 nM) with respect to the total signal (1 mM = 100% of the signal).

centration increases. The analysis in terms of  $f_{\text{rec}}$  evidences, initially, a notable increment in the rectification efficiency with the boric acid concentration (Fig. 3(b)). Then,  $f_{\text{rec}}$  reaches an asymptotic value for [boric acid] > 10<sup>-7</sup> M, *i.e.* the  $f_{\text{rec}}$  values do not appreciably change in the concentration range between 10<sup>-7</sup> M and 10<sup>-3</sup> M of boric acid, which might indicate the saturation of the binding sites on the modified surface. Additionally, in Fig. 3(c), the relative change in the rectification factor ( $f_{\text{rec}}/f_{\text{rec}}^0$ ) in the limits of concentrations can be observed. The PET/SiO<sub>2</sub>-Glu SSN exposure to boric acid solutions with concentrations of 0.1 nM and 0.5 nM increases  $f_{\text{rec}}$  to almost 50% and 100% compared to the initial response, respectively. Furthermore, the relative change to 0.1 nM boric acid concentration represents 14.8% of the total rectification efficiency of the device (Fig. 3(d)). This implied that by using gluconamide moieties as chemical receptors, solid-state nanopores have been engineered to respond to the presence of borate ions under low concentration conditions (sub-nanomolar range) as compared to borate concentrations in thermal spring water (0.47 mM).<sup>94</sup> Or, in other words, the threshold concentration for the borate-driven actuation of the ionic gate is well below the concentration range of practical interest.

In this context, the specific interaction of the glycol moieties and borates was interpreted in terms of a binding model adapted to the case of the iontronic response of SSN.<sup>78</sup> The general binding scheme is presented in Scheme S1.†

Using a binding model similar to the one described by Laucirica *et al.*,<sup>95</sup> the iontronic response was studied in terms of the dissociation equilibrium of boric acid and the subsequent boroester formation with the gluconamide moieties on the surface. Basically, the formation of the boroester between borate ions in solution and gluconamide groups on the channels' surface at working pH depends on the borate concentration in the solution. This binding process has an associated affinity constant,  $K_B$ . Considering this, a simple binding model for the iontronic response of PET/SiO<sub>2</sub>-Glu SSN leads to the following dependence of the rectification factor on the boric acid analytical concentration (see the ESI† for a detailed derivation of eqn (1)):

$$f_{\text{rec}} - f_{\text{rec}}^0 = (f_{\text{rec}}^{\infty} - f_{\text{rec}}^0) \frac{K_B' C_B}{1 + K_B' C_B} \quad (1)$$

where  $f_{\text{rec}}^0$  is the rectification value before borate was added,  $f_{\text{rec}}^{\infty}$  is the value adopted at high concentrations,  $C_B$  is the boric acid analytical concentration, and  $K_B'$  (defined as  $K_B' = \alpha K_B$ )

means an effective binding constant under the operative conditions. Thus,  $K_B$  can be determined by fitting the  $f_{\text{rec}}-f_{\text{rec}}^0$  experimental values as a function of boric acid analytical concentration. As shown in Fig. 3(b), the  $f_{\text{rec}}-f_{\text{rec}}^0$  experimental values are in good agreement with the non-linear dependence predicted by eqn (1). Using the above-described model,  $K_B$  was determined to be  $0.15 \pm 0.1 \text{ nM}^{-1}$ .

On the other hand, it has been reported that the kinetics of the boronate ester formation is fast, especially when the boron atom is found in a tetrahedral environment.<sup>96</sup> Also, as previously mentioned, borate anions form a very stable complex with saccharides, especially with fructose.<sup>86</sup> Taking advantage of this interaction, the modified nanopore was exposed to successive cycles of 100 mM boric acid/100 mM fructose solutions in order to demonstrate the reversibility of the borate–saccharide complex formation. For this aim,  $I$ - $V$  curves were measured and the iontronic behavior was studied in terms of the rectification efficiency (Fig. 4(a)). It was observed that exposure to 100 mM fructose solutions resulted in a significant decrease of the rectification factors, *i.e.*: “OFF” state, which was ascribed to the decrease in the surface charge density as a consequence of the rupture of the saccharide–borate bond in the boronate (Fig. 4(b)). Otherwise, when the nanochannel is exposed to 100 mM boric acid, the system recovers the initial rectification “ON” state. In other words, the boronate complex is formed

again on the pore walls and the negative surface charge density increases. In addition, the analysis of the transient current at +1 V ( $I$  vs. time) evidenced a rapid reversible

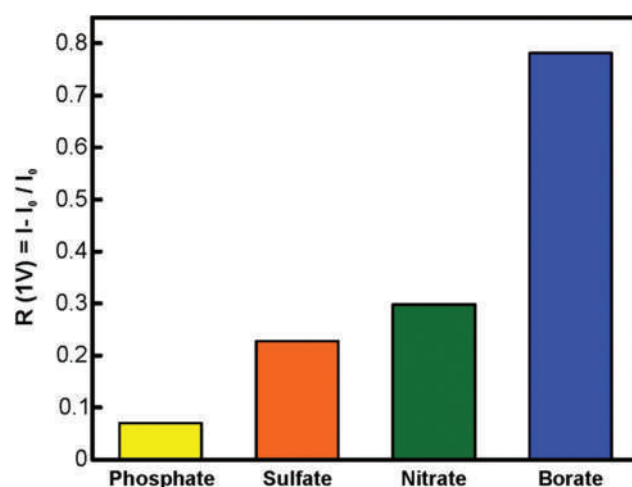


Fig. 5 Selectivity experiments in terms of the ratio of the current change ( $R = (I - I_0) / I_0$ ;  $I$  and  $I_0$  currents were registered at  $V_t = +1 \text{ V}$ ).  $I$ - $V$  curves were measured *in situ* after the addition of 25 mM phosphate, sulfate, nitrate, and borate.

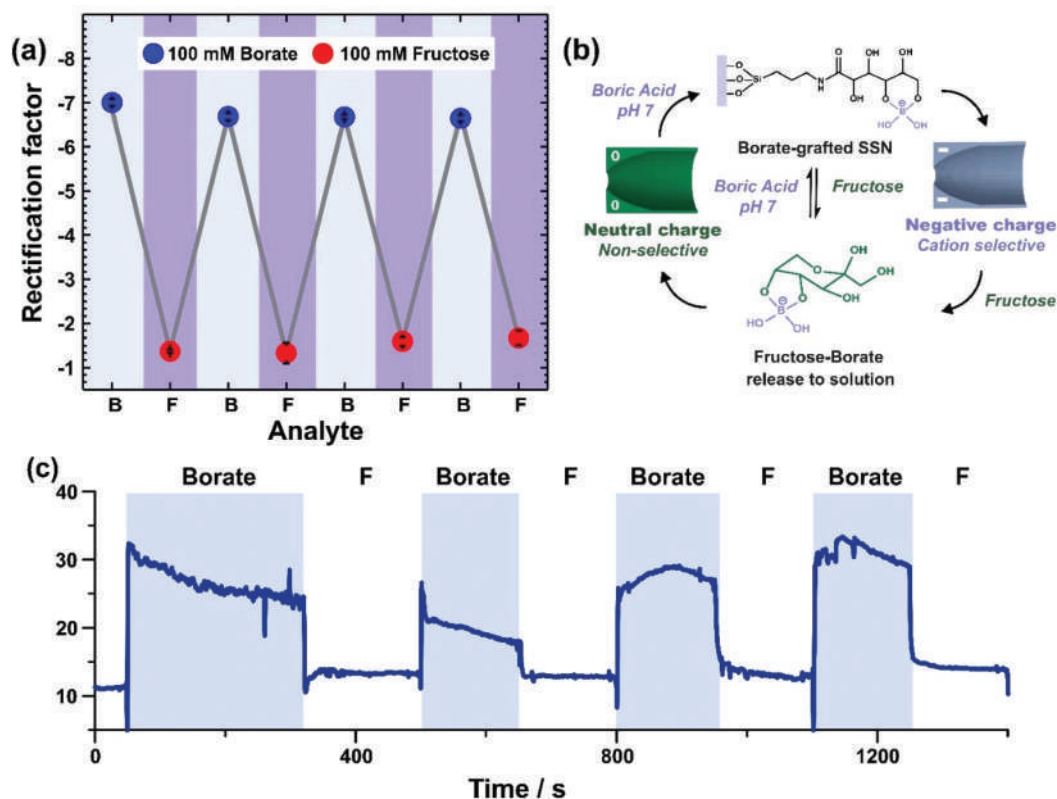


Fig. 4 (a) Reversibility experiment with 100 mM borate (B) and fructose (F) in terms of the rectification factor. (b) Scheme depicting the nanochannel borate–fructose reversibility mechanism. (c) Reversibility experiment with 100 mM borate and fructose (F) in terms of the transient current. All measurements were carried out *in situ* at pH 7.

response of the nanodevice upon the exposure to borate and fructose (Fig. 4(c)). These results demonstrate that the Glu-borate reaction may be an interesting approach to build highly reversible stimuli-responsive devices by exploiting the borate-sugar specific chemistry.

Finally, to explore the selectivity of the PET/SiO<sub>2</sub>-Glu SSN, the effect produced on the ionic transport by interfering analytes was also evaluated. The interfering analytes studied were sulfate, nitrate, and phosphate anions. Each *I*-*V* measurement was performed at the saturation concentration for borate (25 mM). To facilitate the interpretation, selectivity results are shown in terms of the relative current increase, *R*, the respective analyte exposure, being  $R = I - I_0/I_0$ , where *I*<sub>0</sub> is the current before adding the analyte. As can be seen in Fig. 5, sulfate, nitrate, and phosphate anions did not cause significant changes in the iontronic output. In contrast, the presence of borate anions promotes a marked increase in the current change ratio which demonstrates the selective character of the borate-sugar confined interaction in the PET/SiO<sub>2</sub>-Glu SSN.

## Conclusions

In summary, we have designed and developed a borate-responsive nanodevice based on the glyco-silanization of a SiO<sub>2</sub>-coated PET nanochannel obtained by combining both track-etched and atomic layer deposition (ALD) technologies. The successful modification of the channel at each functionalization step was evidenced by the changes in the iontronic output.

To the best of our knowledge, this is the first report that employs silane chemistry on SiO<sub>2</sub> ALD coated PET SSNs to develop ion-responsive switchable ionic gates. The presence of gluconamide moiety groups on the nanochannel surface allowed the modulation of the iontronic signal by exploiting the well-known sugar-borate complexation. Thus, the changes in the surface charge density caused by the saccharide-borate equilibrium formation are transduced to changes in the iontronic output. Then, the nanofluidic device switches from a non-selective iontronic regime ("OFF" state) to a cation-selective iontronic regime ("ON" state) by exposing the modified membrane (PET/SiO<sub>2</sub>-Glu) to borate solutions. In order to explain the borate-responsiveness, we proposed a binding model for describing the interaction between the saccharide groups on the nanochannel walls and borate anions, which satisfactorily fits the dependence of the rectification factors on the borate concentration. Moreover, the iontronic responsiveness was demonstrated to be reversible under successive exposure to borate and fructose solutions. This strategy resulted in the development of a borate-driven nanofluidic actuator capable of controlling the ionic flux through the nanochannel depending on the presence and concentration of borate ions. This approach could be used to engineer feedback-controlled delivery systems for ions or even charged particles. In this context, we believe that these results provide interesting insights into the construction robust ionic gates for

developing nanofluidic integrated circuits and activatable nanofluidic devices and would be applicable for sensing, directed molecular transport and separation, and targeted drug delivery at the nanoscale level.

## Experimental section

### Materials

Synthetic nanochannels were fabricated in PET foils (Hostaphan RN 12, Hoechst) of thickness 12 μm. *N*-(3-Triethoxysilylpropyl) gluconamide (TESPG) 50% in EtOH solution was purchased from ABCR. Boric acid (purity 100%) and HEPES (<99.5%) were purchased from Anedra and Sigma-Aldrich respectively. Potassium chloride (Anedra) was of analytical grade. All reagents were used as received without further purification.

### Fabrication of ALD-coated single pore nanochannel foils

Bullet-shaped single pore nanochannels were prepared on PET membranes by ion-track etching.<sup>89</sup> Firstly, PET foils were irradiated by accelerated Au ions (11.1 MeV per nucleon) at the UNILAC (Universal Linear Accelerator) of GSI, Darmstadt. After that, surfactant-assisted asymmetric etching was carried out yielding bullet-shaped nanochannels.<sup>97</sup> In this method, the base side was soaked in 6 M NaOH, while the tip side was soaked in the same solution with the addition of 0.05% Dowfax 2a1 for 6–7 min at 60 °C. Finally, the membrane was exhaustively washed with pure water. Subsequently, PET foils were coated with SiO<sub>2</sub> (thickness ~10 nm) by applying a defined number of ALD cycles using a self-built ALD system. Details of the ALD setup are described elsewhere.<sup>53</sup> The reactor walls were heated to 60 °C. The precursors were fed into the reactor by setting the valve opening time to 0.1 s for both SiCl<sub>4</sub> (Sigma-Aldrich, 99.9%) and deionised H<sub>2</sub>O. For SiO<sub>2</sub> deposition onto PET membranes, the cyclic ABAB-type ALD process consisted of 1 min exposure to each precursor separated by 1 min intervals of N<sub>2</sub> purging (99.999%, 200 mL min<sup>-1</sup>). Pyridine was used as a catalyst.

### Surface nanochannel modification

The PET/SiO<sub>2</sub> membrane was modified with TESPGE by a typical silanization reaction protocol. Briefly, 250 μL of the commercial sample (~1.3 mmol) was dissolved in 10 mL of ethanol and was left in contact with the PET/SiO<sub>2</sub> membrane overnight at room temperature. Then, the glycol-modified foils (PET/SiO<sub>2</sub>-Glu SSN) were washed with Milli-Q water and dried with N<sub>2</sub>.

### Composition analysis by X-ray photoelectron spectroscopy (XPS)

The PET/SiO<sub>2</sub>-Glu modified foil was characterized by XPS using a VG Microtech ESCA spectrometer with a non-monochromatic Al-K(α) radiation source (300 W, 15 kV,  $h\nu = 1486.6$  eV), combined with a VG-100-AX hemispherical analyzer operating at a 25 eV pass energy. All the XPS spectra were calibrated with reference to the adventitious C 1s peak at 284.8 eV, to rule out

any possible spectral shift due to a charging effect. The chamber pressure was kept at  $<10^{-9}$  Torr during the measurements. A wide range spectrum and the assignment of its characteristic peaks are available in the ESI (Fig. S4(a) and (b)†).

### Preparation of boric acid/borate solutions

Boric acid aqueous solutions of different concentrations (1  $\mu$ M, 1 to 100 mM) were prepared for the conductivity measurements using KCl 0.1 M as the supporting electrolyte and 10 mM HEPES buffer to maintain the pH of the solutions at 7. As shown in Fig. S5(a),† at this pH, there is a small proportion of boric acid as borate anion (boric acid has a pKa of 9.2).<sup>84</sup> Despite this, another simultaneous equilibrium takes place and the borate anion reacts with vicinal diols to form borate esters, and boric acid/borate ion equilibrium is displaced to borate formation (Fig. S5(b)†).

### Conductance measurements

Current–voltage ( $I$ – $V$ ) curves were obtained using a potentiostat (Gamry 600) with a four-electrode set-up (working, working sense, reference, and counter electrode) as reported elsewhere.<sup>98</sup> Measurements were performed in a homemade conductivity cell fabricated to avoid current leakage. Both the reference and working-sense were commercial Ag/AgCl/3 M NaCl electrodes, while the working and counter electrodes were Pt wires. For all the experiments, the working electrode was placed at the tip side of the membrane, while the counter electrode was placed at the base side to ensure a facile interpretation of the results. For the  $I$ – $V$  measurements, the voltage was swept between  $-1$  V and  $+1$  V at a scan rate of  $100$  V  $s^{-1}$ . Additionally, conductivity measurements for the analytes (boric acid/borate, fructose, sulfate, nitrate, and phosphate) were performed by filling the cell with the corresponding solution in the same buffer and after a stabilization time (10 minutes), new  $I$ – $V$  curves were measured in the presence of the analyte. Then, the membrane was washed with deionized water and employed for the next analyte.

### Rectification factor ( $f_{\text{rec}}$ )

To correlate the changes in the  $I$ – $V$  curves with the surface charge density of the nanochannel, the rectification efficiency was quantified employing a rectification factor ( $f_{\text{rec}}$ ). For the cation-driven regime (negatively charged surface), the rectification factor can be computed as:

$$f_{\text{rec}} = -|I(1 \text{ V})/I(-1 \text{ V})| \quad (2)$$

where the current in the numerator is the largest current value corresponding to the higher conductance state (positive transmembrane voltage limit), while the one in the denominator is the lowest current value corresponding to the lower conductance state (negative transmembrane voltage limit).<sup>29</sup>

### Contact angle measurements

In all cases (PET/SiO<sub>2</sub>, PET/SiO<sub>2</sub>–Glu, PET/SiO<sub>2</sub>–Glu borate treated SSNs), contact angles (CA) were measured using a

Ramé-Hart goniometer (Model 290) by dispensing 1  $\mu$ L droplets of 0.1 M KCl in 10 mM HEPES (pH 7). The reported values correspond to the average of five independent measurements. After measuring the CA of PET/SiO<sub>2</sub>–Glu SSN, the foil was treated with 100 mM boric acid in 0.1 M KCl and 10 mM HEPES solution (pH 7) for 10 minutes to obtain PET/SiO<sub>2</sub>–Glu SSN treated with borate. The foil was then washed with deionized water and its CA was measured with the protocol specified above.

## Conflicts of interest

There are no conflicts to declare.

## Acknowledgements

V. M. C. acknowledges the postdoctoral financial support from Universidad Nacional de La Plata. Y. T. T. and G. L. acknowledge the scholarship from CONICET. G. L. also acknowledges a scholarship for a research stay from DAAD and the support of the get\_involved programme of the GSI. M. L. C., G. P. M., W. A. M., and O. A. acknowledge the financial support from Universidad Nacional de La Plata (PPID-X867), CONICET (PIP-0370) and ANPCyT (PICT-2017-1523 and PICT2016-1680). C. T. and M. E. T. M. acknowledge support from the LOEWE project iNAPO funded by the Hessen State Ministry of Higher Education, Research and Arts. The irradiated PET foils are part of the experiment UMAT, which was performed at the beam line X0 at the GSI Helmhottzentrum für Schwerionenforschung, Darmstadt (Germany) in the frame of FAIR Phase-0. Access to XPS facilities at INFAP was granted by Sistema Nacional de rayos X (SNRX), Ministerio de Ciencia, Tecnología e Innovación de La Nación Argentina.

## References

- 1 G. Pérez-Mitta, M. E. Toimil-Molares, C. Trautmann, W. A. Marmisollé and O. Azzaroni, *Adv. Mater.*, 2019, **31**, 1901483.
- 2 Z. Long, S. Zhan, P. Gao, Y. Wang, X. Lou and F. Xia, *Anal. Chem.*, 2018, **90**, 577–588.
- 3 M. Lepoitevin, T. Ma, M. Bechelany, J.-M. Janot and S. Balme, *Adv. Colloid Interface Sci.*, 2017, **250**, 195–213.
- 4 Z. Zhang, L. Wen and L. Jiang, *Chem. Soc. Rev.*, 2018, **47**, 322–356.
- 5 G. Pérez-Mitta, A. G. Albesa, C. Trautmann, M. E. Toimil-Molares and O. Azzaroni, *Chem. Sci.*, 2017, **8**, 890–913.
- 6 B. Hille, *Ion Channels of Excitable Membranes*, Sinauer Associates, Sunderland, Massachusetts U.S.A, 3rd edn, 2001.
- 7 G. Pérez-Mitta, A. S. Peinetti, M. L. Cortez, M. E. Toimil-Molares, C. Trautmann and O. Azzaroni, *Nano Lett.*, 2018, **18**, 3303–3310.

- 8 K. Xiao, Y. Zhou, X.-Y. Kong, G. Xie, P. Li, Z. Zhang, L. Wen and L. Jiang, *ACS Nano*, 2016, **10**, 9703–9709.
- 9 B. Vilozny, P. Actis, R. A. Seger and N. Pourmand, *ACS Nano*, 2011, **5**, 3191–3197.
- 10 D. Al Sulaiman, P. Cadinu, A. P. Ivanov, J. B. Edel and S. Ladame, *Nano Lett.*, 2018, **18**, 6084–6093.
- 11 K. J. Freedman, L. M. Otto, A. P. Ivanov, A. Barik, S.-H. Oh and J. B. Edel, *Nat. Commun.*, 2016, **7**, 10217.
- 12 P. Ramírez, P. Y. Apel, J. Cervera and S. Mafé, *Nanotechnology*, 2008, **19**, 315707.
- 13 R. Li, X. Fan, Z. Liu and J. Zhai, *Adv. Mater.*, 2017, **29**, 1702983.
- 14 P. Y. Apel, I. V. Blonskaya, O. L. Orelovitch, P. Ramirez and B. A. Sartowska, *Nanotechnology*, 2011, **22**, 175302.
- 15 Y. Lin, Y.-L. Ying, R. Gao and Y.-T. Long, *Chem. – Eur. J.*, 2018, **24**, 13064–13071.
- 16 S. Chen, Y. Tang, K. Zhan, D. Sun and X. Hou, *Nano Today*, 2018, **20**, 84–100.
- 17 M. Wang, H. Meng, D. Wang, Y. Yin, P. Stroeve, Y. Zhang, Z. Sheng, B. Chen, K. Zhan and X. Hou, *Adv. Mater.*, 2019, **31**, 1805130.
- 18 B. Niu, K. Xiao, X. Huang, Z. Zhang, X.-Y. Kong, Z. Wang, L. Wen and L. Jiang, *ACS Appl. Mater. Interfaces*, 2018, **10**, 22632–22639.
- 19 J. Gao, W. Guo, D. Feng, H. Wang, D. Zhao and L. Jiang, *J. Am. Chem. Soc.*, 2014, **136**, 12265–12272.
- 20 A. Seidenstücker, S. Beirle, F. Enderle, P. Ziemann, O. Marti and A. Plettl, *Beilstein J. Nanotechnol.*, 2018, **9**, 1390–1398.
- 21 P. Actis, A. C. Mak and N. Pourmand, *Bioanal. Rev.*, 2010, **1**, 177–185.
- 22 M. Ali, B. Yameen, R. Neumann, W. Ensinger, W. Knoll and O. Azzaroni, *J. Am. Chem. Soc.*, 2008, **130**, 16351–16357.
- 23 M. Ali, B. Yameen, J. Cervera, P. Ramírez, R. Neumann, W. Ensinger, W. Knoll and O. Azzaroni, *J. Am. Chem. Soc.*, 2010, **132**, 8338–8348.
- 24 G. Pérez-Mitta, W. A. Marmisollé, C. Trautmann, M. E. Toimil-Molares and O. Azzaroni, *J. Am. Chem. Soc.*, 2015, **137**, 15382–15385.
- 25 B. Yameen, M. Ali, M. Álvarez, R. Neumann, W. Ensinger, W. Knoll and O. Azzaroni, *Polym. Chem.*, 2010, **1**, 183–192.
- 26 G. Pérez-Mitta, L. Burr, J. S. Tuninetti, C. Trautmann, M. E. Toimil-Molares and O. Azzaroni, *Nanoscale*, 2016, **8**, 1470–1478.
- 27 G. Pérez-Mitta, W. A. Marmisollé, C. Trautmann, M. E. Toimil-Molares and O. Azzaroni, *Adv. Mater.*, 2017, **29**, 1–6.
- 28 G. Pérez-Mitta, J. S. Tuninetti, W. Knoll, C. Trautmann, M. E. Toimil-Molares and O. Azzaroni, *J. Am. Chem. Soc.*, 2015, **137**, 6011–6017.
- 29 G. Pérez-Mitta, A. Albesa, F. M. Gilles, M. E. Toimil-Molares, C. Trautmann and O. Azzaroni, *J. Phys. Chem. C*, 2017, **121**, 9070–9076.
- 30 B. Yameen, M. Ali, R. Neumann, W. Ensinger, W. Knoll and O. Azzaroni, *Nano Lett.*, 2009, **9**, 2788–2793.
- 31 G. Pérez-Mitta, A. G. Albesa, M. E. Toimil Molares, C. Trautmann and O. Azzaroni, *ChemPhysChem*, 2016, **17**, 2718–2725.
- 32 G. Laucirica, Y. Toum Terrones, V. M. Cayón, M. L. Cortez, M. E. Toimil-Molares, C. Trautmann, W. A. Marmisollé and O. Azzaroni, *Nanoscale*, 2020, **12**, 18390–18399.
- 33 G. Pérez-Mitta, W. A. Marmisollé, A. G. Albesa, M. E. Toimil-Molares, C. Trautmann and O. Azzaroni, *Small*, 2018, **1702131**, 1–8.
- 34 Q. Liu, K. Xiao, L. Wen, Y. Dong, G. Xie, Z. Zhang, Z. Bo and L. Jiang, *ACS Nano*, 2014, **8**, 12292–12299.
- 35 Z. S. Siwy, M. R. Powell, A. Petrov, E. Kalman, C. Trautmann and R. S. Eisenberg, *Nano Lett.*, 2006, **6**, 1729–1734.
- 36 G. Pérez-Mitta, A. G. Albesa, W. Knoll, C. Trautmann, M. E. Toimil-Molares and O. Azzaroni, *Nanoscale*, 2015, **7**, 15594–15598.
- 37 B. Yameen, M. Ali, R. Neumann, W. Ensinger, W. Knoll and O. Azzaroni, *Small*, 2009, **5**, 1287–1291.
- 38 W. Guo, H. Xia, F. Xia, X. Hou, L. Cao, L. Wang, J. Xue, G. Zhang, Y. Song, D. Zhu, Y. Wang and L. Jiang, *ChemPhysChem*, 2010, **11**, 859–864.
- 39 M. Zhang, X. Hou, J. Wang, Y. Tian, X. Fan, J. Zhai and L. Jiang, *Adv. Mater.*, 2012, **24**, 2424–2428.
- 40 P. Li, G. Xie, X.-Y. Kong, Z. Zhang, K. Xiao, L. Wen and L. Jiang, *Angew. Chem., Int. Ed.*, 2016, **55**, 15637–15641.
- 41 R. Spohr, *Ion tracks and microtechnology*, Vieweg+Teubner Verlag, 1990.
- 42 I. Vlasiouk, S. Smirnov and Z. Siwy, *ACS Nano*, 2008, **2**, 1589–1602.
- 43 Z. Siwy, P. Apel, D. Dobrev, R. Neumann, R. Spohr, C. Trautmann and K. Voss, *Nucl. Instrum. Methods Phys. Res., Sect. B*, 2003, **208**, 143–148.
- 44 E. B. Kalman, I. Vlasiouk and Z. S. Siwy, *Adv. Mater.*, 2008, **20**, 293–297.
- 45 Y. Ai, J. Liu, B. Zhang and S. Qian, *Sens. Actuators, B*, 2011, **157**, 742–751.
- 46 J.-H. Han, K. B. Kim, H. C. Kim and T. D. Chung, *Angew. Chem.*, 2009, **121**, 3888–3891.
- 47 J.-H. Han, K. B. Kim, J. H. Bae, B. J. Kim, C. M. Kang, H. C. Kim and T. D. Chung, *Small*, 2011, **7**, 2629–2639.
- 48 N. Rampazzo, E. Genovese, D. Palomba, F. Prodi and L. Zaccaroni, *Methods Appl. Fluoresc.*, 2018, **6**, 022002.
- 49 P. F. Hockl, A. Wolosiuk, J. M. Pérez-Sáez, A. V. Bordoni, D. O. Croci, Y. Toum-Terrones, G. J. A. A. Soler-Illia and G. A. Rabinovich, *Pharmacol. Res.*, 2016, **109**, 45–54.
- 50 S. M. George, *Chem. Rev.*, 2010, **110**, 111–131.
- 51 J. W. Elam, D. Routkevitch, P. P. Mardilovich and S. M. George, *Chem. Mater.*, 2003, **15**, 3507–3517.
- 52 M. S. Sander, M. J. Côté, W. Gu, B. M. Kile and C. P. Tripp, *Adv. Mater.*, 2004, **16**, 2052–2057.
- 53 A. Spende, N. Sobel, M. Lukas, R. Zierold, J. C. Riedl, L. Gura, I. Schubert, J. M. M. Moreno, K. Nielsch, B. Stühn, C. Hess, C. Trautmann and M. E. Toimil-Molares, *Nanotechnology*, 2015, **26**(33), 335301.

- 54 B. Kumari, D. John, P. Hoffmann, A. Spende, M. E. Toimil-Molares, C. Trautmann, C. Hess, P. Ruff, M. Schulze, R. Stark, G. Buntkowsky, A. Andrieu-Brunsen and T. Gutmann, *Z. Phys. Chem.*, 2018, **232**, 1173–1186.
- 55 S. Onclin, B. J. Ravoo and D. N. Reinhoudt, *Angew. Chem., Int. Ed.*, 2005, **44**, 6282–6304.
- 56 C. J. Brinker and G. W. Scherer, *Sol-gel science : the physics and chemistry of sol-gel processing*, Academic Press, 1990.
- 57 M. Ma, *Crit. Rev. Biochem. Mol. Biol.*, 2007, **42**, 463–480.
- 58 S. Zhao, Y.-B. Zheng, S.-L. Cai, Y.-H. Weng, S.-H. Cao, J.-L. Yang and Y.-Q. Li, *Electrochem. Commun.*, 2013, **36**, 71–74.
- 59 L.-X. Zhang, X.-H. Cao, Y.-B. Zheng and Y.-Q. Li, *Electrochem. Commun.*, 2010, **12**, 1249–1252.
- 60 T. Kudo and A. Nakajima, *Appl. Phys. Lett.*, 2012, **100**, 2012–2015.
- 61 A. Nakajima, *Appl. Sci.*, 2016, **6**, 94.
- 62 S. Agnihotri, S. Mukherji and S. Mukherji, *Nanoscale*, 2013, **5**, 7328.
- 63 W. Lee, T. Kang, S.-H. Kim and J. Jeong, *Sensors*, 2018, **18**, 307.
- 64 D. Lewandowski, D. Bajerlein and G. Schroeder, *Struct. Chem.*, 2014, **25**, 1505–1512.
- 65 U. Arslan, *J. Phytopathol.*, 2016, **164**, 678–685.
- 66 R. B. Goldbloom and A. Goldbloom, *J. Pediatr.*, 1953, **43**, 631–643.
- 67 D. G. Cochran, *Experientia*, 1995, **51**, 561–563.
- 68 D. Li, Y. Chen and Z. Liu, *Chem. Soc. Rev.*, 2015, **44**, 8097–8123.
- 69 J. Tang, Y. Liu, D. Qi, G. Yao, C. Deng and X. Zhang, *Proteomics*, 2009, **9**, 5046–5055.
- 70 J. Kamcev, M. K. Taylor, D. Shin, N. N. Jarenwattananon, K. A. Colwell and J. R. Long, *Adv. Mater.*, 2019, **31**, 1808027.
- 71 G. Kaupp, M. R. Naimi-Jamal and V. Stepanenko, *Chem. – Eur. J.*, 2003, **9**, 4156–4161.
- 72 S. Liu, J. Pan, J. Liu, Y. Ma, F. Qiu, L. Mei, X. Zeng and G. Pan, *Small*, 2018, **14**, 1703968.
- 73 D. Wen, W. Liu, A.-K. Herrmann, D. Haubold, M. Holzschuh, F. Simon and A. Eychmüller, *Small*, 2016, **12**, 2439–2442.
- 74 M. Lee, S.-H. Lee, I.-K. Oh and H. Lee, *Small*, 2017, **13**, 1600443.
- 75 D.-E. Wang, J. Yan, J. Jiang, X. Liu, C. Tian, J. Xu, M.-S. Yuan, X. Han and J. Wang, *Nanoscale*, 2018, **10**, 4570–4578.
- 76 A. Adameczyk-Woźniak, M. Jakubczyk, A. Sporzyński and G. Żukowska, *Inorg. Chem. Commun.*, 2011, **14**, 1753–1755.
- 77 Y. Jiang and Y. Ma, *Anal. Chem.*, 2009, **81**, 6474–6480.
- 78 A. Schneider, J. Hemmerlé, M. Allais, J. Didierjean, M. Michel, M. D'Ischia and V. Ball, *ACS Appl. Mater. Interfaces*, 2018, **10**, 7574–7580.
- 79 A. Larcher, A. Lebrun, M. Smietana and D. Laurencin, *New J. Chem.*, 2018, **42**, 2815–2823.
- 80 W. Wang, X. Gao and B. Wang, *Curr. Org. Chem.*, 2002, **6**, 1285–1317.
- 81 T. D. James and S. Shinkai, in *Artificial Receptors as Chemosensors for Carbohydrates*, ed. S. Penadés, Springer Berlin Heidelberg, Berlin, Heidelberg, 2002, pp. 159–200.
- 82 V. Kochkodan, N. Bin Darwish and N. Hilal, The Chemistry of Boron in Water, in *Boron Separation Processes*, ed. N. Kabay, M. Bryjak and N. Hilal, Elsevier, Amsterdam, 1st edn, 2015, ch. 2, pp. 35–63.
- 83 J. Yan, H. Fang and B. Wang, *Med. Res. Rev.*, 2005, **25**, 490–520.
- 84 E. Aznar, C. Coll, M. D. Marcos, R. Martínez-Máñez, F. Sancenón, J. Soto, P. Amorós, J. Cano and E. Ruiz, *Chem. – Eur. J.*, 2009, **15**, 6877–6888.
- 85 G. Pérez-Mitta, W. A. Marmisollé, A. G. Albesa, M. E. Toimil-Molares, C. Trautmann and O. Azzaroni, *Small*, 2018, **14**, 1702131.
- 86 J. F. Verchere and M. Hlaibi, *Polyhedron*, 1987, **6**, 1415–1420.
- 87 E. Aznar, M. D. Marcos, R. Martínez-Máñez, F. Sancenón, J. Soto, P. Amorós and C. Guillem, *J. Am. Chem. Soc.*, 2009, **131**, 6833–6843.
- 88 I. Candel, E. Aznar, L. Mondragón, C. de la Torre, R. Martínez-Máñez, F. Sancenón, M. D. Marcos, P. Amorós, C. Guillem, E. Pérez-Payá, A. Costero, S. Gil and M. Parra, *Nanoscale*, 2012, **4**, 7237.
- 89 P. Y. Apel, I. V. Blonskaya, S. N. Dmitriev, O. L. Orelovitch, A. Presz and B. A. Sartowska, *Nanotechnology*, 2007, **18**, 305302.
- 90 G. Laucirica, M. E. Toimil-Molares, C. Trautmann, W. Marmisollé and O. Azzaroni, *ACS Appl. Mater. Interfaces*, 2020, **12**, 28148–28157.
- 91 G. Laucirica, A. Albesa, M. E. Toimil-Molares, C. Trautmann, W. Marmisollé and O. Azzaroni, *Nano Energy*, 2020, 104612.
- 92 R. M. Almeida, C. G. Pantano and M. A. Rui, *J. Appl. Phys.*, 1990, **68**, 4225–4232.
- 93 M. Pálmai, L. N. Nagy, J. Mihály, Z. Varga, G. Tárkányi, R. Mizsei, I. C. Szigyártó, T. Kiss, T. Kremmer and A. Bóta, *J. Colloid Interface Sci.*, 2013, **390**, 34–40.
- 94 A. Tapparo and G. Giorgio Bombi, *Analyst*, 1998, **123**, 1771–1773.
- 95 G. Laucirica, G. Pérez-Mitta, M. E. Toimil-Molares, C. Trautmann, W. A. Marmisollé and O. Azzaroni, *J. Phys. Chem. C*, 2019, **123**, 28997–29007.
- 96 S. L. Wiskur, J. J. Lavigne, H. Ait-Haddou, V. Lynch, Y. H. Chiu, J. W. Canary and E. V. Anslyn, *Org. Lett.*, 2001, **3**, 1311–1314.
- 97 P. Y. Apel, I. V. Blonskaya, N. V. Levkovich and O. L. Orelovich, *Pet. Chem.*, 2011, **51**, 555–567.
- 98 G. Laucirica, W. A. Marmisollé, M. E. Toimil-Molares, C. Trautmann and O. Azzaroni, *ACS Appl. Mater. Interfaces*, 2019, **11**, 30001–30009.